Geochemical Perspectives Letters

Testing *ab initio* garnet-clinopyroxene Ca-isotope fractionation models with natural data

J. Munro[1*], J.C. Lassiter[1], J.D. Barnes[1], A.M. Satkoski[1]

OPEN ACCESS

https://doi.org/10.7185/geochemlet.2549

Abstract

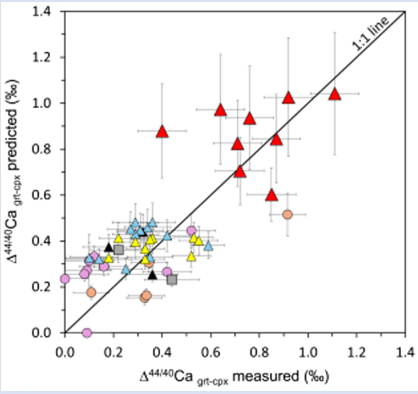

Calcium stable isotope variations help track processes from melt generation to crustal recycling in the mantle, but applying this system requires understanding of inter-mineral and mineral-melt isotopic fractionation. Density functional theory (DFT) models have been used to constrain Ca-isotope fractionation between garnet and clinopyroxene as a function of temperature, pressure, and composition, because garnet can strongly fractionate Ca. However, experimental and empirical data to test DFT predictions for equilibrium $\Delta^{44/40}Ca_{grt\text{-}cpx}$ remain limited. We measured $\delta^{44/40}Ca$ values of clinopyroxene and garnet from eclogite xenoliths in the Navajo Volcanic Field, Colorado Plateau (USA). Combining these low-temperature samples with higher-temperature literature data, we find $\Delta^{44/40}Ca_{grt\text{-}cpx}$ is correlated with $10^6/T^2$ ($\Delta^{44/40}Ca_{grt\text{-}cpx} = 0.63 \times 10^6/T^2$). No correlations were found with mineral composition after correcting for temperature, and pressure is not expected to have a significant effect. To first order, DFT model predictions agree well with observed trends in natural samples.

Received 7 August 2025 | Accepted 6 November 2025 | Published 4 December 2025

Introduction

Mantle peridotites exhibit limited variation in $\delta^{44/40}Ca$ ($\delta^{44/40}Ca = [(^{44}Ca/^{40}Ca)_{sample}/(^{44}Ca/^{40}Ca)_{SRM915a} - 1] \times 1000$; *e.g.*, Dai *et al.*, 2020), but Ca isotopes are significantly fractionated during surface processes (He *et al.*, 2023 and references therein). Consequently, Ca isotopes have been utilised as tracers for recycled material and proxies for carbonate cycling in the mantle, especially when considering low-$\delta^{44/40}Ca$ basalts or carbonatites (Kang *et al.*, 2016, 2017; Chen *et al.*, 2023; Li *et al.*, 2024; Zhu *et al.*, 2025). However, this view is challenged by a broad negative correlation between $\delta^{44/40}Ca$ and La/Lu observed in mid-ocean ridge basalts (MORB) and ocean island basalts (OIB; Eriksen and Jacobsen, 2022 and references therein). Because garnet strongly fractionates both Ca isotopes and heavy REE, this correlation may reflect isotopic fractionation during melting of garnet-bearing lithologies (Eriksen *et al.*, 2024). In contrast, clinopyroxene-melt fractionation produces melts with $\delta^{44/40}Ca$ values only <0.1 ‰ lower than spinel peridotites (Eriksen and Jacobsen, 2022; Chen *et al.*, 2024). Parameterising garnet-clinopyroxene fractionation is therefore necessary to model the effects of melting of garnet-bearing sources on melt $\delta^{44/40}Ca$, better enabling us to distinguish contributions from equilibrium melting, sedimentary recycling and disequilibrium processes on the $\delta^{44/40}Ca$ of xenoliths and mantle-derived melts.

To characterise the behaviour of calcium isotopes during equilibrium fractionation, studies have focused on identifying the primary factors, such as temperature (Antonelli *et al.*, 2019; Li *et al.*, 2022), pressure (Chen *et al.*, 2020; Li *et al.*, 2022) and mineral composition (Antonelli *et al.*, 2019; Chen *et al.*, 2020), that control inter-mineral or mineral-melt isotopic fractionation. Modelling the effects of these parameters is essential to constrain the $\delta^{44/40}Ca$ variation generated during igneous and metamorphic processes under isotopic equilibrium (Li *et al.*, 2025). However, to date, most studies have relied on theoretical *ab initio* modelling (Antonelli *et al.*, 2019; Chen *et al.*, 2020; Li *et al.*, 2022; Xiao *et al.*, 2022), with limited use of natural or experimental samples to validate model predictions (Smart *et al.*, 2021; Li *et al.*, 2022, 2025). Furthermore, the few natural samples analysed have predominantly come from South African kimberlite localities (Roberts Victor, Chen *et al.*, 2020; Li *et al.*, 2022; Bellsbank, Smart *et al.*, 2021; and Premier, Tappe *et al.*, 2021), which equilibrated at high temperatures (>800 °C). Hence, the temperature dependence of Ca-isotope fractionation has not yet been adequately tested.

We present new mineral $\delta^{44/40}Ca$ data for a suite of low-temperature eclogites from the Navajo Volcanic Field (NVF) in the Colorado Plateau, USA. These results are combined with existing garnet and clinopyroxene $\delta^{44/40}Ca$ from natural samples to test first-principles $\delta^{44/40}Ca$ fractionation models. We evaluate the proposed factors controlling garnet-clinopyroxene Ca-isotope fractionation, and consider the implications for $\delta^{44/40}Ca$ fractionation during partial melting.

Sample Description Results

Eclogitic xenoliths ($n = 9$) from Garnet Ridge ultramafic diatreme were selected from the NVF xenolith collection at the University of Texas at Austin (UT-Austin). They are subrounded nodules

1. Department of Earth and Planetary Sciences, University of Texas at Austin, Austin, Texas, United States of America
* Corresponding author (email: joshua.munro@utexas.edu)

approximately 2 to 4.5 cm in diameter, dominated by jadeite-rich pyroxene, almandine-rich garnet, with lawsonite and zoisite (Table S-1). Garnet and clinopyroxene major element compositions were determined by electron microprobe (Table S-2) for Mg-Fe garnet-clinopyroxene thermometry. Calcium isotope data were collected at UT-Austin. See Supplementary Information for method details. Garnet $\delta^{44/40}$Ca values range from 1.54 to 1.98 ‰ and pyroxenes vary from 0.76 to 1.21 ‰, with $\delta^{44/40}$Ca fractionation ($\Delta^{44/40}Ca_{grt\text{-}cpx} = \delta^{44/40}Ca_{garnet} - \delta^{44/40}Ca_{clinopyroxene}$) values of 0.64 to 1.11 ‰ (Table S-3).

Discussion

Comparison of natural data to Ca-isotope fractionation models. Density functional theory (DFT) models predict that Ca-isotope fractionation is primarily controlled by Ca-O bond strength, with vibrational frequencies and force constants influencing bond stiffness and thus isotope partitioning (Schauble, 2004; Antonelli *et al.*, 2019; Li *et al.*, 2022; Xiao *et al.*, 2022). Equilibrium fractionation arises from vibrational zero-point energy differences and partition functions, in which heavier isotopes preferentially occupy sites with stiffer bonds (*e.g.*, Schauble, 2004). Fractionation is proportional to $1/T^2$ because increasing temperature results in a smaller difference in vibrational energy between two phases. Because mineral composition variation affects lattice structure, this also influences Ca-O bond length and $\Delta^{44/40}Ca_{grt\text{-}cpx}$ (*e.g.*, Antonelli *et al.*, 2019). This effect is predicted to be greater in garnet than in clinopyroxene because the garnet lattice is more rigid and therefore more affected by cation substitutions than the comparatively flexible pyroxene lattice (Antonelli *et al.*, 2019; Li *et al.*, 2022).

The accuracy of DFT models depends on theoretical assumptions, such as the choice of vibration energy model or functional (Local Density Approximation *vs.* Generalised Gradient Approximation), lattice framework chosen, choice of mineral endmembers, and parameters chosen for adjustment (*e.g.*, composition or pressure; Li *et al.*, 2025). Due to computational limitations, models are generally run for compositional endmembers rather than complex solid solutions. Uncertainties in vibrational frequency inputs and use of different approaches or software can introduce systematic errors (Li *et al.*, 2025), which may produce discrepancies between empirical data and *ab initio* predictions. Systematic errors within approaches may be cancelled out when using the same models for a mineral pair, but unpredictable errors may occur when approaches from different papers are combined (Li *et al.*, 2025).

To test whether first-principles models accurately predict isotopic fractionation in natural samples, we present $\Delta^{44/40}Ca_{grt\text{-}cpx}$ from this and previous studies against $10^6/T^2$ (Fig. 1). To ensure estimated temperatures are internally consistent, we apply the same garnet-clinopyroxene Mg-Fe thermometer procedure to all NVF and literature samples (see Supplementary Information). The natural data are compared to DFT models from Antonelli *et al.* (2019), Li *et al.* (2022) and Xiao *et al.* (2022). The shaded regions show the model ranges for: Antonelli *et al.* (2019), where garnet almandine-grossular-pyrope composition is varied and clinopyroxene is fixed as diopside; Li *et al.* (2022), bound by their 0 and 10 GPa pyrope-diopside models; and Xiao *et al.* (2022), in which the garnet is fixed as almandine, and jadeite type changes with variable Na + Al substitution for Ca + Mg.

The weighted regression of all the natural data yields the following line:

$$\Delta^{44/40}Ca_{grt\text{-}cpx} = 1.44(\pm0.15) \times 10^6/T^2 - 0.51(\pm0.09), \quad \text{Eq. 1}$$

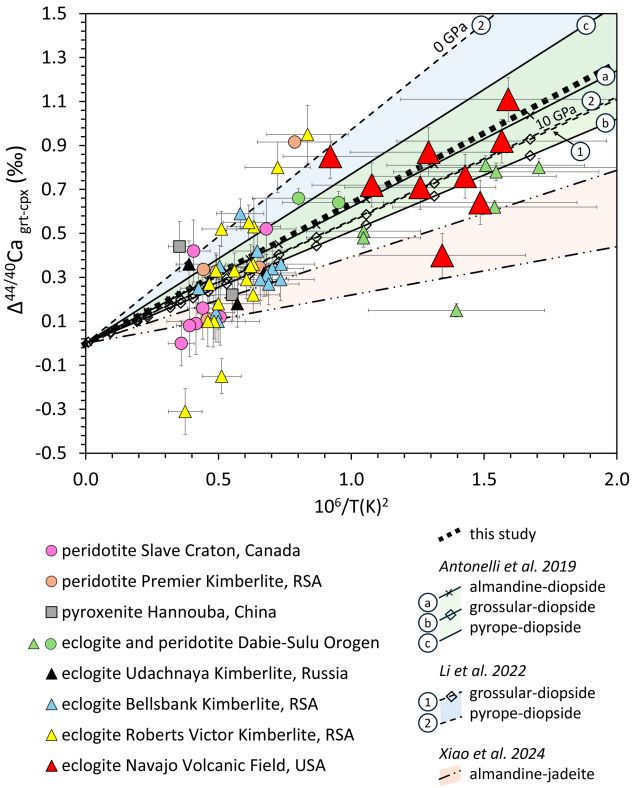

Figure 1 $\Delta^{44/40}Ca_{grt\text{-}cpx}$ plotted against $1/T^2$ for the samples in this study and previous work (see text). Natural data for eclogites (triangles), peridotites (circles) and pyroxenites (squares) are compared to DFT models by Antonelli *et al.* (2019), Li *et al.* (2022) and Xiao *et al.* (2022). All temperatures recalculated following the protocol described in Supplementary Information. Error bars represent 2 s.e., some are smaller than symbols. The Li *et al.* (2022) grossular-diopside and 10 GPa pyrope-diopside lines overlap.

with a mean squared weighted deviation (MSWD) of 7.5 ($n = 65$). The slope of this fractionation line is significantly greater than DFT predictions, and the intercept is non-zero, inconsistent with models. Li *et al.* (2022) noted that Type II Roberts Victor samples ('unmetasomatised') form a steeply dipping array (increasing $\Delta^{44/40}Ca_{grt\text{-}cpx}$ with $10^6/T^2$) and contain samples with $\Delta^{44/40}Ca_{grt\text{-}cpx} < 0$, inconsistent with model predictions. It is unclear whether this is a disequilibrium process (Antonelli *et al.*, 2019), pressure effect (Chen *et al.*, 2020), due to jadeite/high-pressure garnet that have since destabilised (Li *et al.*, 2022), or a mixture of processes. Because the Ca-isotope equilibrium of those samples is debated, they are excluded, reducing the MSWD to 6.4 and bringing the regression more in line with predictions (see Eq. S-2).

Additionally, we note that the only *in situ* samples are from the Dabie-Sulu Orogen, which has undergone slow exhumation (Hacker *et al.*, 2006). Mg-Fe diffusion is more rapid and continues to lower temperatures than Ca diffusion (Ganguly, 2010). Hence, these slowly-cooled samples are expected to have $T_{Mg\text{-}Fe}$ less than T_{Ca}. Because the $T_{Mg\text{-}Fe}$ is expected to not be in equilibrium with $\Delta^{44/40}Ca_{grt\text{-}cpx}$, these samples are also not suited to this analysis. Removing Dabie-Sulu samples from the regression improves the MSWD to 5.7 (Eq. S-3). A final consideration is the non-zero intercept – DFT modelling and thermodynamics predict that $\Delta^{44/40}Ca_{grt\text{-}cpx}$ converges to 0 as T approaches infinity (Schauble, 2004). Because no sign reversal is anticipated for Ca-isotope fractionation of garnet and clinopyroxene, the regression is forced to the intercept. The heavy dashed line is the weighted

regression of all natural data, excluding Dabie-Sulu and Type II Roberts Victor (Fig. 1). The revised empirical, temperature-dependent model is now:

$$\Delta^{44/40}Ca_{grt\text{-}cpx} = 0.63(\pm 0.03) \times 10^6/T^2. \quad \text{Eq. 2}$$

This model is consistent with DFT predictions, as the slope is within the range of Antonelli *et al.* (2019) and slightly higher than the slopes of 0.567 from Huang *et al.* (2019) and 0.52 from Li *et al.* (2025). Increasing $\Delta^{44/40}Ca_{grt\text{-}cpx}$ fractionation is correlated with decreasing temperature (increasing $10^6/T^2$; MSWD = 6.8, $n = 49$, $p < 0.001$). The NVF eclogites, which have lower temperature estimates (~500 to 800 °C; Table S-5) than most literature samples (~900 to 1200 °C), have higher $\Delta^{44/40}Ca_{grt\text{-}cpx}$, as predicted.

By using the average garnet composition for all samples ($Py_{47}Alm_{34}Grs_{18}$) to linearly mix the Antonelli *et al.* (2019) pyrope-, almandine- and grossular-diopside models, one obtains a model indistinguishable from Equation 2 (slope = 0.64). Hence, to a first order, DFT modelling accurately predicts natural observations.

Constraining controls on natural $\Delta^{44/40}Ca_{grt\text{-}cpx}$ variability. Despite the similarity between the empirical and DFT models, the natural samples show significant scatter from the regression (Fig. 1 and Fig. S-5), which may be due to analytical error, or reflect the influence of factors such as pressure (Chen *et al.*, 2020), garnet composition (Chen *et al.*, 2020; Li *et al.*, 2022), pyroxene composition (Wang *et al.*, 2019; Li *et al.*, 2022; Xiao *et al.*, 2022), or disequilibrium effects (Antonelli *et al.*, 2019). To test the influence of these parameters, the departure of natural samples from the regression is quantified using residuals (measured $\Delta^{44/40}Ca_{grt\text{-}cpx}$ − predicted $\Delta^{44/40}Ca_{grt\text{-}cpx}$). The linear regression (Eq. 2) is used to calculate the predicted $\Delta^{44/40}Ca_{grt\text{-}cpx}$ from temperature estimates for each sample, and the residuals are then compared to compositional parameters and pressure estimates (Fig. 2) to assess correlations.

First, though, it is worth testing whether the scatter is due to random errors. The residuals are compared to the normal distribution of expected errors from thermometric uncertainty, isotopic measurement error and error in the linear regression (average total $2\sigma = 0.14$ ‰; Fig. 3). The true residual 2σ is 0.34 ‰. Hence, while some departures may be due to uncertainty in Mg-Fe exchange thermometry and measured $\Delta^{44/40}Ca_{grt\text{-}cpx}$, most scatter is unaccounted for.

Varying garnet composition from grossular to almandine to pyrope is predicted to increase $\Delta^{44/40}Ca_{grt\text{-}cpx}$ (Antonelli *et al.*, 2019) because these cation substitutions decrease the Ca-O bond length, but we do not observe correlations between residuals and garnet almandine, grossular, or pyrope content (grossular shown; Fig. 2). However, at high temperatures (>1000 K) the compositional effect is expected to be <0.2 ‰ (*e.g.*, Li *et al.*, 2025), similar to the propagated measurement errors, and so compositional effects may not be easily observable given other sources of scatter. It is clear, however, that for a given temperature, $\Delta^{44/40}Ca_{grt\text{-}cpx}$ varies more than is predicted for compositional variation (Fig. 2).

Due to similar ionic sizes, Mg-Fe substitution does not significantly alter the pyroxene lattice size. Hence, no Ca-O bond length change (or $\Delta^{44/40}Ca_{grt\text{-}cpx}$ effect) is expected. Consistent with this, there is no clear correlation between residuals and diopside content, as noted by Li *et al.* (2025). A correlation between $\Delta^{44/40}Ca_{grt\text{-}cpx}$ and jadeite content was previously reported for Dabie-Sulu eclogites (Wang *et al.*, 2019), and DFT modelling by Xiao *et al.* (2022) predicts $\Delta^{44/40}Ca_{grt\text{-}cpx}$ changes depending on how Na + Al is substituted in jadeite. However,

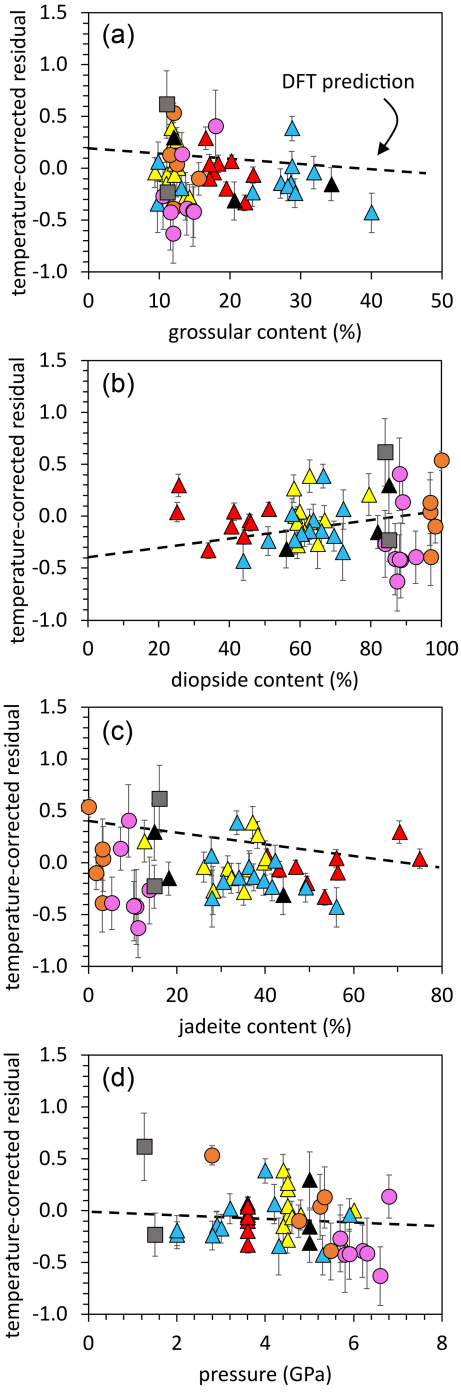

Figure 2 Plots of temperature-corrected $\Delta^{44/40}Ca_{grt\text{-}cpx}$ residuals against **(a)** garnet grossular content, **(b)** pyroxene diopside content, **(c)** pyroxene jadeite content, and **(d)** pressure estimates. Symbols as for Figure 1.

neither Chen *et al.* (2020) nor Smart *et al.* (2021) observed $\Delta^{44/40}Ca_{grt\text{-}cpx}$ correlations with jadeite content in mantle eclogites. Similarly, no correlation is seen with the global dataset of $\Delta^{44/40}Ca_{grt\text{-}cpx}$ residuals and jadeite content (Fig. 2). Therefore, clinopyroxene composition does not detectably influence $\Delta^{44/40}Ca_{grt\text{-}cpx}$.

Clinopyroxene lattice structure is more compressible than that of garnet and is predicted to have shorter Ca-O bond lengths at greater pressures, increasing uptake of ^{44}Ca into clinopyroxene and reducing $\Delta^{44/40}Ca_{grt\text{-}cpx}$. Chen *et al.* (2020) determined pressure estimates and $\Delta^{44/40}Ca_{grt\text{-}cpx}$ for Roberts

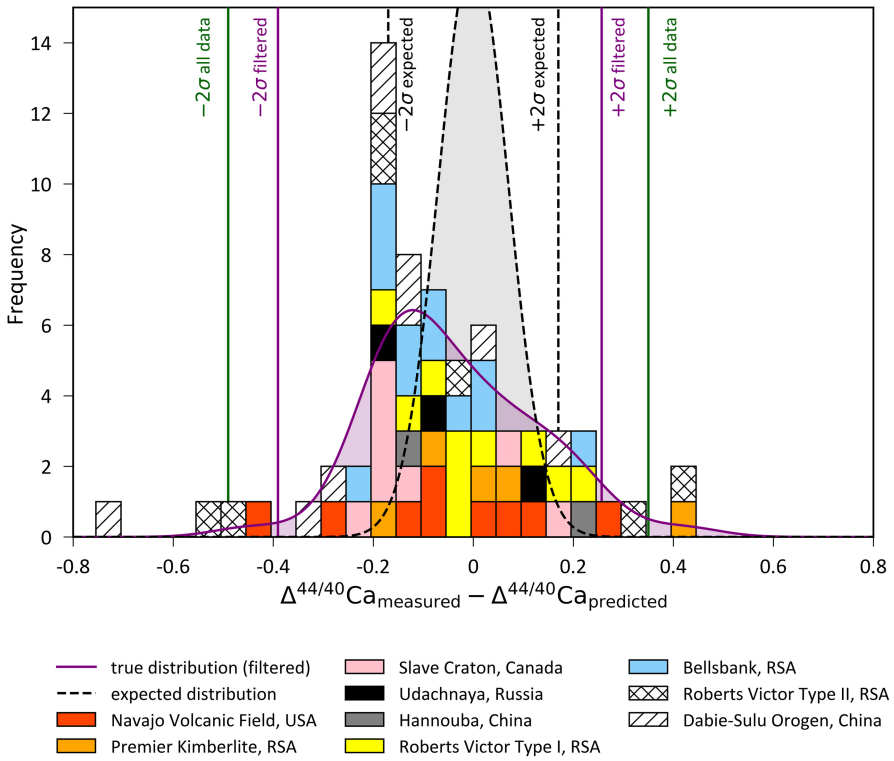

Figure 3 Histogram of $\Delta^{44/40}Ca_{grt\text{-}cpx}$ residuals, and error distribution expected from the predicted $\Delta^{44/40}Ca_{grt\text{-}cpx}$ and $1/T^2$ uncertainty (dashed lines) compared to the actual distribution of filtered residuals (purple lines; excluded Dabie-Sulu or Roberts Victor Type II).

Victor eclogites to infer that Ca fractionation decreases by 0.3 ‰ over 3 to 4.5 GPa (1000 K). However, *ab initio* modelling by Li *et al.* (2022, 2025) suggests garnet and clinopyroxene lattices are equally affected by pressure, yielding pressure-induced $\Delta^{44/40}Ca_{grt\text{-}cpx}$ variation of <0.05 ‰ at 1000 K. Significant pressure effects do occur when garnet Ca concentration is very low (<1 wt. %, pyrope-diopside models; Li *et al.*, 2022), but most natural samples examined have Ca as a major element (up to 20 wt. %). We do not observe a correlation between the $\Delta^{44/40}Ca_{grt\text{-}cpx}$ residuals of natural samples and estimated published pressures (Fig. 2). It is not possible to clearly assess the pressure effect with current data because the pressure estimates are based on the Mg-Fe thermometry, and *vice versa*, but recent models predict small effects.

Some unexplained scatter is likely due to disequilibrium (*e.g.*, subsolidus Ca-isotope diffusion) or a mismatch between Ca and Mg-Fe closure temperatures. Overall, no clear signs of disequilibrium were observed when examining garnet-clinopyroxene Mg, Ti and REE partitioning (see Supplementary Information). Because rapid Mg-Fe diffusion continues to lower temperatures than Ca, where samples cooled slowly as for *in situ* Dabie-Sulu samples, the Mg-Fe temperature estimates are likely lower than the Ca-isotope closure temperature. This would result in overestimation of the predicted $\Delta^{44/40}Ca_{grt\text{-}cpx}$ so that residuals would be shifted to negative values. If the sample was rapidly heated, *i.e.* during eruption, Mg-Fe temperature may be reset to higher temperatures, whereas the Ca-isotope temperatures may remain unperturbed, producing the opposite shift in residuals. There is evidence of temperature inconsistencies when REE and Mg-Fe thermometry are compared (Fig. S-3), and this may be a major contributor to the broader than expected error distribution. Unfortunately, no garnet-clinopyroxene Ca geothermometer exists, but the Mg-Fe thermometers are the most accessible and widely used method, generally producing a reasonable approximation to the Ca-isotope temperature for rapidly exhumed samples.

Although disequilibrium processes (*e.g.*, diffusion) likely affect some samples, most natural samples are close to equilibrium, within the current ability to determine temperature and $\Delta^{44/40}Ca_{grt\text{-}cpx}$. General disequilibrium processes are unlikely to dominate during processes such as melt generation.

Ca-isotope variation in basalts. Ocean island basalts span a wider $\delta^{44/40}Ca$ range and extend to lower values than MORB (Eriksen and Jacobsen, 2022). There is debate whether Ca-isotope variations in MORB and OIB primarily reflect variations in source composition (*e.g.*, incorporation of recycled components; Huang *et al.*, 2011), isotopic fractionation variations due to melting of garnet-rich and garnet-poor lithologies (*e.g.*, Dai *et al.*, 2020), or disequilibrium fractionation during melt generation (*e.g.*, kinetic effects; Antonelli *et al.*, 2019; Li *et al.*, 2025). Eriksen *et al.* (2024) and Eriksen and Jacobsen (2022) suggest the OIB $\delta^{44/40}Ca$ correlation with La/Lu reflects mixing of melts derived from garnet-rich and garnet-poor lithologies, but also suggest involvement of recycling and source enrichment. Whereas previous studies used DFT models to constrain inter-mineral and mineral-melt isotopic fractionation, our study provides independent confirmation of DFT estimates using natural samples.

Using the clinopyroxene-melt Ca-isotope fractionation of Li *et al.* (2025) and Equation 2, we model the $\delta^{44/40}Ca$ range likely generated during melting of spinel peridotite, garnet peridotite, and garnet-dominated lithologies (*e.g.*, garnetite or rodingite). The observed OIB $\delta^{44/40}Ca$ range is unlikely to simply reflect mixing of melts from garnet and spinel peridotite, assuming a starting peridotite composition of ~0.94 ‰ (Fig. 4). Assuming equal modal abundances of garnet and clinopyroxene, results show that partial melting of garnet peridotite (or eclogite) does not generate melts with $\delta^{44/40}Ca < 0.78$ ‰. Even melting of pure

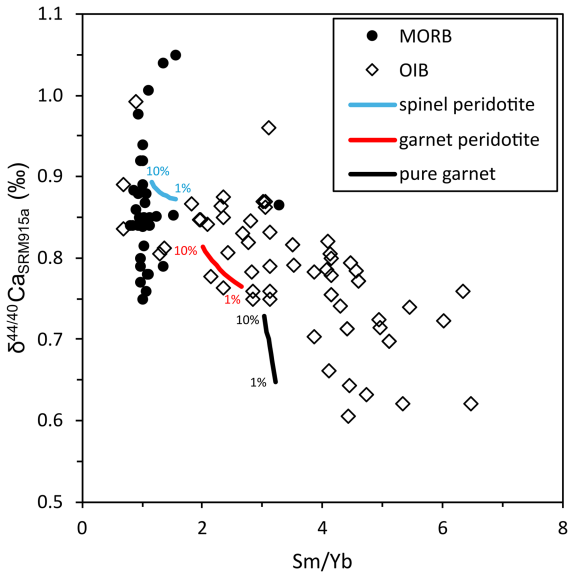

Figure 4 Comparison of $\delta^{44/40}$Ca *versus* Sm/Yb for MORB (Erikson and Jacobsen, 2022) and OIB (Eriksen *et al.*, 2024). Lines represent batch melting of a spinel peridotite, garnet peridotite or pure garnet source, with 1 to 10 % partial melting.

garnet lithologies cannot generate melts with $\delta^{44/40}$Ca < 0.69 ‰. Thus, the lowest observed OIB $\delta^{44/40}$Ca (high La/Lu and Sm/Yb) likely derive from anomalously low-$\delta^{44/40}$Ca sources, possibly due to incorporation of recycled carbonates or prior metasomatism by melts derived from garnet-bearing sources. Additionally, the global correlation observed between $\delta^{44/40}$Ca and La/Lu and Sr and Nd isotopes (Eriksen *et al.*, 2024) suggests that variation in source composition, rather than disequilibrium fractionation, is responsible for generating the large OIB $\delta^{44/40}$Ca range.

Acknowledgements

The authors are grateful to D. Smith for curating the UT-Austin NVF collection and sharing samples, the Navajo Nation for permission to collect on their land, K.S. Befus and A.V. Mott for assistance in obtaining electron microprobe analyses, and C. Sun for valuable discussions. The efficient editorial handling by R. Tartèse and constructive reviews of E. Schauble and an anonymous reviewer are greatly appreciated. This work was supported by a National Science Foundation (NSF) grant to JDB and JCL (#2234385) and Geological Society of America (GSA) Lipman Student Research Grant to JM.

Editor: Romain Tartèse

Additional Information

Supplementary Information accompanies this letter at https://www.geochemicalperspectivesletters.org/article2549.

Cite this letter as: Munro, J., Lassiter, J.C., Barnes, J.D., Satkoski, A.M. (2025) Testing *ab initio* garnet-clinopyroxene Ca-isotope fractionation models with natural data. *Geochem. Persp. Let.* 38, 11–16. https://doi.org/10.7185/geochemlet.2549

References

Antonelli, M.A., Schiller, M., Schauble, E.A., Mittal, T., DePaolo, D.J., Chacko, T., Grew, E.S., Tripoli, B. (2019) Kinetic and equilibrium Ca isotope effects in high-T rocks and minerals. *Earth and Planetary Science Letters* 517, 71–82. https://doi.org/10.1016/j.epsl.2019.04.013

Chen, C., Huang, J.-X., Foley, S.F., Wang, Z., Moynier, F., Liu, Y., Dai, W., Li, M. (2020) Compositional and pressure controls on calcium and magnesium isotope fractionation in magmatic systems. *Geochimica et Cosmochimica Acta* 290, 257–270. https://doi.org/10.1016/j.gca.2020.09.006

Chen, C., Foley, S.F., Tappe, S., Ren, H., Feng, L., Liu, Y. (2024) Calcium isotopes track volatile components in the mantle sources of alkaline rocks and associated carbonatites. *Earth and Planetary Science Letters* 625, 118489. https://doi.org/10.1016/j.epsl.2023.118489

Chen, Q., Zhou, M.-F., Xia, X.-P., Liu, P.-P. (2023) Li and O isotopes of mantle xenoliths from deep fault-related Cenozoic basalts in eastern China: The role of subducted components in the generation of the heterogeneous lithospheric mantle. *Chemical Geology* 628, 121471. https://doi.org/10.1016/j.chemgeo.2023.121471

Dai, W., Wang, Z., Liu, Y., Chen, C., Zong, K., Zhou, L., Zhang, G., Li, M., Moynier, F., Hu, Z. (2020) Calcium isotope compositions of mantle pyroxenites. *Geochimica et Cosmochimica Acta* 270, 144–159. https://doi.org/10.1016/j.gca.2019.11.024

Eriksen, Z.T., Jacobsen, S.B. (2022) Calcium isotope constraints on OIB and MORB petrogenesis: The importance of melt mixing. *Earth and Planetary Science Letters* 593, 117665. https://doi.org/10.1016/j.epsl.2022.117665

Eriksen, Z.T., Jacobsen, S.B., Day, J.M.D., White, W.M. (2024) Calcium isotope variability among ocean islands reveals the physical and lithological controls on mantle partial melting. *Geochimica et Cosmochimica Acta* 373, 326–341. https://doi.org/10.1016/j.gca.2024.02.011

Ganguly, J. (2010) Cation Diffusion Kinetics in Aluminosilicate Garnets and Geological Applications. *Reviews in Mineralogy and Geochemistry* 72, 559–601. https://doi.org/10.2138/rmg.2010.72.12

Hacker, B.R., Wallis, S.R., Ratschbacher, L., Grove, M., Gehrels, G. (2006) High-temperature geochronology constraints on the tectonic history and architecture of the ultrahigh-pressure Dabie-Sulu Orogen. *Tectonics* 25, TC5006. https://doi.org/10.1029/2005TC001937

He, D., Liu, Y., Moynier, F., Foley, S.F., Chen, C., Zhu, Y., Lü, X., Zhang, G., Zong, K. (2023) Tightly coupled Ca-Zn-Sr isotope co-variations in basalts caused by recycled calcium carbonate in the mantle source. *Chemical Geology* 637, 121678. https://doi.org/10.1016/j.chemgeo.2023.121678

Huang, S., Farkaš, J., Jacobsen, S.B. (2011) Stable calcium isotopic compositions of Hawaiian shield lavas: Evidence for recycling of ancient marine carbonates into the mantle. *Geochimica et Cosmochimica Acta* 75, 4987–4997. https://doi.org/10.1016/j.gca.2011.06.010

Huang, F., Zhou, C., Wang, W., Kang, J., Wu, Z. (2019) First-principles calculations of equilibrium Ca isotope fractionation: Implications for oldhamite formation and evolution of lunar magma ocean. *Earth and Planetary Science Letters* 510, 153–160. https://doi.org/10.1016/j.epsl.2018.12.034

Kang, J.-T., Zhu, H.-L., Liu, Y.-F., Liu, F., Wu, F., Hao, Y.-T., Zhi, X.-C., Zhang, Z.-F., Huang, F. (2016) Calcium isotopic composition of mantle xenoliths and minerals from Eastern China. *Geochimica et Cosmochimica Acta* 174, 335–344. https://doi.org/10.1016/j.gca.2015.11.039

Kang, J.-T., Ionov, D.A., Liu, F., Zhang, C.-L., Golovin, A.V, Qin, L.-P., Zhang, Z.-F., Huang, F. (2017) Calcium isotopic fractionation in mantle peridotites by melting and metasomatism and Ca isotope composition of the Bulk Silicate Earth. *Earth and Planetary Science Letters* 474, 128–137. https://doi.org/10.1016/j.epsl.2017.05.035

Li, J.-L., Wang, X.-S., Wang, Z., Huang, J., Gao, J. (2024) Ca–Zn isotope fractionation during fluid–rock interaction in subduction zones and its implication for deep carbon cycle. *Chemical Geology* 670, 122425. https://doi.org/10.1016/j.chemgeo.2024.122425

Li, Y., Wu, Z., Huang, S., Wang, W. (2022) Pressure and concentration effects on intermineral calcium isotope fractionation involving garnet. *Chemical Geology* 591, 120722. https://doi.org/10.1016/j.chemgeo.2022.120722

Li, Y., Hardin, J., Wang, W., Wu, Z., Huang, S. (2025) Mineral-melt calcium isotope fractionation factors constrained using *ab initio* molecular dynamics simulations and their implications to calcium isotope effects during partial

melting in the upper mantle. *Geochimica et Cosmochimica Acta* 396, 51–70. https://doi.org/10.1016/j.gca.2025.02.032

Schauble, E.A. (2004) Applying Stable Isotope Fractionation Theory to New Systems. *Reviews in Mineralogy and Geochemistry* 55, 65–111. https://doi.org/10.2138/gsrmg.55.1.65

Smart, K.A., Tappe, S., Woodland, A.B., Greyling, D.R., Harris, C., Gussone, N. (2021) Constraints on Archean crust recycling and the origin of mantle redox variability from the $\delta^{44/40}$Ca – δ^{18}O – fO_2 signatures of cratonic eclogites. *Earth and Planetary Science Letters* 556, 116720. https://doi.org/10.1016/j.epsl.2020.116720

Tappe, S., Massuyeau, M., Smart, K.A., Woodland, A.B., Gussone, N., Milne, S., Stracke, A. (2021) Sheared Peridotite and Megacryst Formation Beneath the Kaapvaal Craton: a Snapshot of Tectonomagmatic Processes across the Lithosphere–Asthenosphere Transition. *Journal of Petrology* 62, egab046. https://doi.org/10.1093/petrology/egab046

Wang, Y., He, Y., Wu, H., Zhu, C., Huang, S., Huang, J. (2019) Calcium isotope fractionation during crustal melting and magma differentiation: Granitoid and mineral-pair perspectives. *Geochimica et Cosmochimica Acta* 259, 37–52. https://doi.org/10.1016/j.gca.2019.05.030

Xiao, Z.-C., Zhou, C., Kang, J.-T., Wu, Z.-Q., Huang, F. (2022) The factors controlling equilibrium inter-mineral Ca isotope fractionation: Insights from first-principles calculations. *Geochimica et Cosmochimica Acta* 333, 373–389. https://doi.org/10.1016/j.gca.2022.07.021

Zhu, H., Shan, Y., Liao, R., Zhang, L., Deng, J., Li, C., Du, L., Zhang, Z., Sun, W. (2025) Ca-Sr-Nd isotopic signatures of mid-ocean ridge basalts from the Central Indian Ridge and implications for recycled materials in the Indian Ocean mantle domain. *Chemical Geology* 673, 122546. https://doi.org/10.1016/j.chemgeo.2024.122546